Modelling of Steel-Concrete Composite Structures in Fire Using OpenSees

Modelling of Steel-Concrete Composite Structures in Fire Using OpenSees

Jian Jiang[1,*], Asif Usmani[2] and Guo-Qiang Li[3]

[1]College of Civil Engineering, Tongji University, Shanghai 200092, China
[2]School of Engineering, the University of Edinburgh, Edinburgh EH9 3JF, United Kingdom
[3]State Key Laboratory for Disaster Reduction in Civil Engineering, Tongji University, Shanghai 200092, China

(Received: 27 February 2013; Received revised form: 23 December 2013; Accepted: 10 January 2014)

Abstract: This paper presents the extension of the structural analysis software framework OpenSees for modeling steel framed composite structures subjected to fire including the development of a geometrically nonlinear shell element. The new shell element is formed by a combination of membrane elements and Mindlin plate bending elements using a general total Lagrangian formulation. The MITC technique (Mixed Interpolation of Tensorial Components) is applied to alleviate shear locking problems and the addition of drilling degrees of freedom is included. A new thermal load class was created to define the temperature distribution through the thickness of the shell section. The two-dimensional OpenSees material, DruckerPrager, was modified to model the concrete in the composite deck slab at elevated temperature with temperature-dependent material properties according to the Eurocode 2. A three-dimensional finite element model of a composite structure was built in OpenSees, consisting of a flat reinforced concrete slab modeled by the developed shell element as well as concrete ribs and beams/columns modeled by three-dimensional beam elements. These components were connected by rigid link elements to model composite action. The performance of the developed model is verified and validated by a series of analytical solutions and experimental results respectively. Among these are: one-way bending of steel plates; fire tests on simply supported composite beams; and reinforced concrete slabs where membrane actions are investigated. Cardington restrained beam test and British Steel Corner test are also modeled. The reasonable agreement achieved between OpenSees predictions and experimental measurements shows the validity of the developed OpenSees extension to model composite structures in fire. The horizontal displacement of the column at floor level was modeled for the first time with reasonable agreement. This work is part of a wider project which, upon completion, will provide a user-friendly open-source computational platform for structural fire engineering analyses from fire dynamic simulation through to heat transfer analysis and mechanical analysis.

Key words: OpenSees, composite structures in fire, geometric nonlinearity, shell element, Cardington tests.

1. INTRODUCTION

Since the Broadgate Phase 8 fire in London and the subsequent Cardington fire tests researchers have fully investigated and understood the behavior of whole composite steel-framed concrete structures in fire. The Cardington test results (Huang *et al*. 2000a; Usmani 2000) have confirmed that steel members in real multi-story buildings have significantly greater fire resistance than isolated members in the standard fire test. Spurred on by the Cardington tests and other laboratory tests (Dong *et al*. 2009; Guo and Bailey 2011; Guo 2012), numerous numerical models have been developed in parallel with development of special-purpose finite element program such as ADAPTIC (Izzuddin 1991),

* Corresponding author. Email address: jiangjian_0131@163.com; Tel: +86-21-65977946.

VULCAN (Bailey 1995; Huang *et al*. 1999) and SAFIR (Franssen 2000) developed by researchers at Imperial College, the University of Sheffield and the University of Liege (Belgium), respectively.

Rose *et al*. (1998) published one of the first 3D models of the Cardington tests which showed good agreement between predicted and test deflections for the restrained beam test, corner test and plane frame test. The Reissner-Mindlin plate theory was employed by Bailey (1995) to model the behavior of composite building frames in fire. Based on Bailey's work Huang *et al*. (1999) proposed a nonlinear layered finite element procedure for predicting the structural response of reinforced concrete slabs subjected to fire. Huang *et al*. (2000b) extended the layered procedure (Huang *et al*. 1999) to include the orthotropic properties of composite slabs by introducing an effective stiffness approach. A three-dimensional, nonlinear finite element procedure for modeling composite steel-framed buildings in fire was presented by Huang *et al*. (2000c). The proposed model was an assembly of beam-column, spring, and layered flat shell elements. Numerical simulation of two Cardington tests, restrained beam and corner test, were undertaken using ADAPTIC by Elghazouli *et al*. (2000) and Elghazouli and Izzuddin (2001). A grillage representation of the composite floor was used in which all slab and beam components were represented by beam-column elements. Izzuddin *et al*. (2004) pointed out that previous studies had focused on solving the difficulty arising from modeling the geometric orthotropy of composite slabs by 2D shell elements and classified them into two main approaches. The first approach employed geometric simplification, where uniform thickness shell elements are used with an effective stiffness approach to approximate the influence of the geometric orthotropy (Huang *et al*. 2000b). The second approach employed dimensional simplification, where a grillage 1D element was used to approximate the 2D bending and membrane response (Elghazouli *et al*. 2000; Elghazouli and Izzuddin 2001). In contrast to the previous grillage beam-column elements, Izzuddin *et al*. (2004) introduced a new flat shell element for ribbed composite slabs accounting for geometric and material nonlinearities. The proposed element can deal with the geometric orthotropy of composite floor by means of incorporating two additional displacement fields corresponding to stretching and shear modes in the rib region.

The effects of geometric nonlinearity were ignored in the early analyses of concrete slabs subjected to fire. For accurate determination of large displacement and membrane action exhibited by concrete slabs in fire, the layered procedures previously developed (Huang *et al*. 1999, 2000c) were extended to include geometric nonlinearity based on a total Lagrangian approach (Huang *et al*. 2003a, b). This geometrically nonlinear model was later used to model composite concrete floors by Huang *et al*. (2004). Yu *et al*. (2008) presented a new model for orthotropic slabs in fire by assembly of a 9-node solid slab element and 3-node beam element. Recently, Huang (2010) extended the previous layered procedure (Huang *et al*. 2003a, b) to take into account the effects of concrete spalling on both thermal and structural behavior of concrete slabs in fire.

The research team in the University of Edinburgh used the commercial finite element package ABAQUS to model the Cardington tests and obtain an extensive and in-depth understanding of the structural behavior of the composite steel-framed buildings under fire conditions (Sanad *et al*. 2000; Gillie *et al*. 2001 2002). For 3D thermomechanical analysis of structures subjected to random fires in ABAQUS, a heat transfer analysis must be carried out on a mesh of continuum solid elements to establish the temperature evolution on sufficient points in the structure. The same mesh can of course be used for simulating the mechanical response. This however is a very computational expensive approach and also not very accurate compared to the much more accurate structural elements (beam-column or frame). However if the analyst chooses to use structural elements, currently ABAQUS only allows five temperature points on the cross-section of a 3D beam-column element. This makes an accurate analysis of the heat transfer meaningless as the temperature resolution obtained is not usable in a structural frame model. Based on the limitation in our use of ABAQUS, a more suitable software platform OpenSees (McKenna 1997; Archer *et al*. 1999; McKenna *et al*. 2010; Mazzoni *et al*. 007) was chosen and extended for modeling structures in fire which also offered excellent capabilities of simulating structural response to earthquakes thus opening the possibility of a multi-hazard simulation capability in OpenSees, e.g. fire following an earthquake (Sharma *et al*. 2012).

This paper presents an augmentation of OpenSees to enable three-dimensional analysis of steel-framed composite structures. A new geometrically nonlinear shell element ShellMITC4GNThermal was developed in OpenSees using a general total Lagrangian formulation. This new shell element is a layered four-node isoparametric element including the drilling degrees of freedom formed by the combination of a membrane element and a Mindlin plate bending element. The MITC technique (Mixed Interpolation of

Tensorial Components) (Dvorkin and Bathe 1984; Bathe and Dvorkin 1986) was applied to alleviate shear locking problems. A new thermal load class ShellThermalAction was developed to define the temperature distribution in the shell element. The existing two-dimensional material class in OpenSees, DruckerPrager (Drucker and Prager 1952), was modified to model concrete slabs at elevated temperature. A three-dimensional finite element model of composite frames then built using OpenSees. The newly developed geometrically nonlinear shell element was used to model the concrete slab and three-dimensional beam elements for modeling concrete ribs and beam/columns. The performance of the proposed model was verified and validated comparing model results against analytical solutions and experimental results, such as: cylindrical bending of plain concrete slabs; composite beams in fire; and reinforced concrete slabs at ambient and elevated temperatures with membrane action. In addition, two Cardington tests (the restrained beam test and the corner test) were modeled and the vertical deflection of slab and beams as well as horizontal displacement of internal and edge columns were output to highlight the behavior of composite structures exposed to fire.

2. OPENSEES MODEL

The OpenSees framework has recently been developed by the authors (with other colleagues) for modelling the behavior of structures in fire (Jiang 2012; Jiang et al. 2013; Jiang and Usmani 2013). The extended two-dimensional modeling capability for structures in fire was included in the OpenSees release 2.4.0 in October 2012. The ultimate aim of the development of OpenSees is to provide a complete and fully automated software framework for the fire load and the associated heat transfer to structural elements and the structural response. This paper focuses on the mechanical behavior of structures under pre-defined temperature distributions. The extensions involve creating a new thermal load pattern class and modifying existing material, section and element classes to include temperature dependency.

For the three-dimensional beam/column elements, a thermal load class Beam3dThermalAction was created to store the temperature distribution in members, this was classified as an elemental load. The storage of temperatures was defined through the beam section by coordinate (LocY, LocZ) in the two directions and the corresponding temperature (T). At this stage a total of 2, 5 and 9 temperature points are available in each direction, respectively (Jiang *et al*. 2013). New temperature dependent material classes for steel and concrete (Steel01Thermal and Concrete02Thermal (Jiang 2012)) were derived by modifying the existing corresponding material classes (McKenna *et al*. 2007) according to Eurocodes. Opensees supports both distributed plasticity and concentrated plasticity based Euler-Bernoulli beam-column elements. Moreover, the distributed plasticity beam-column elements can be classified into the typical displacement-based (DispBeamColumn) and force-based beam-column elements (ForceBeamColumn) (Spacone and Filippou 1992). Both these two beam/column elements have been modified to include temperature related interfaces (DispBeamColumn3dThermal and ForceBeamColumn3dThermal). For a full description of the class hierarchy of new classes added in OpenSees the reader can refer to (Jiang *et al*. 2012).

For modelling concrete slabs, a new geometrically nonlinear shell element ShellMITC4GNThermal is developed based on modification of the existing shell element in OpenSees. These modifications followed the Total Lagrangian procedure with a simplified Green strain. The details of the formation of the shell element is presented in the following section. The class hierarchy of the developed classes is shown in Figure 1. Similar to Beam3dThermalAction, a new thermal load class ShellThermalAction, containing the temperature distribution in slabs, was developed. At this stage the temperature distribution in the plane of slabs is assumed to be uniform and varies only through the thickness. The temperature of each shell layer will be determined by interpolating the temperature at the nearest temperature points according to its location. A thermal load pattern ThermalLoadPattern was developed to define detailed and highly varying time-dependent temperature distributions in structural members where the temperature distributions are retrieved from the thermal load class ShellThermalAction. It can be used as an interface to transfer the temperature distribution from the heat transfer model to the structural model where the structural responses will be predicted. The thermal analysis and structural analysis is uncoupled in OpenSees so far which means that temperature distribution along the element should be provided as input before the structural analysis. Parallel work is progressing on automatically generating time varying structural temperature inputs from a heat transfer analysis within OpenSees (Usmani *et al*. 2012) however direct inputs will always be required for modelling of experiments. A series of parameters containing time points and corresponding temperature for the nine temperature points along the height of the section respectively are defined as the input of the

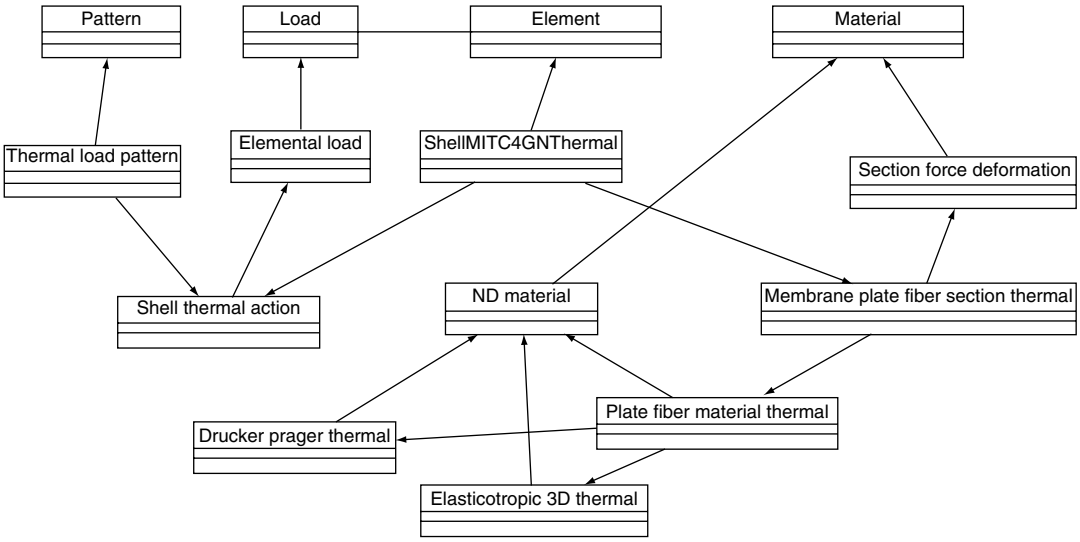

Figure 1. Class diagram for thermomechanical analysis in OpenSees

ThermalLoadPattern class. The maximum temperature at each temperature point through the whole fire duration will be defined first and the temperature can then be defined as a ratio of its absolute value to the corresponding maximum temperature. This scheme can accommodate both heating and cooling scenarios.

Temperature dependent material classes DruckerPragerThermal and section class MembranePlateFiberSectionThermal were developed based on the corresponding classes in OpenSees. The class DruckerPragerThermal was developed to model concrete slabs consisting of the Drucker-Prager yield criterion and a tension cut-off model (Drucker and Prager 1952; Cook *et al*. 2002; Chen and Saleeb 994). The temperature dependent properties are set according to Eurocode 2 (2005). The two-dimensional material class PlateFiberMaterialThermal works as a wrapper class responsible for passing messages between material objects and section objects. The flow chart of element state determination of the extended OpenSees model can be found in reference (Jiang and Usmani 2013).

There are still very few universally acceptable theoretical models available for the constitutive modelling of concrete subject to biaxial states of stress at elevated temperatures. The approach adopted in this paper for constitutive modelling of concrete at elevated temperatures is only an initial attempt which will need to be further refined as more comprehensive data becomes available, especially with respect to the biaxial failure envelope used and the tensile stress–strain curve.

A three-dimensional finite element model can then be set up in OpenSees as shown in Figure 2. The uniform thickness part of the concrete slab is modelled by the developed shell element and the concrete slab ribs and

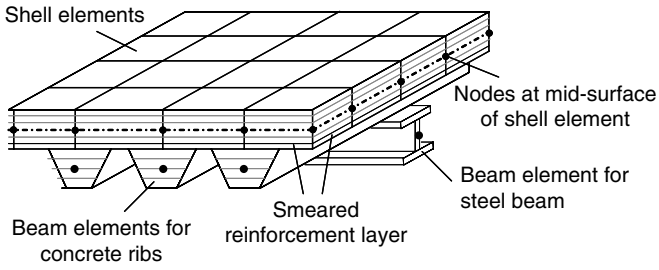

Figure 2. Schematic of OpenSees model for composite structures

steel I beam are modelled by 3D beam elements. These components are connected using rigid link elements (Cook *et al*. 2002). Two rigid-link types "bar" and "beam" are offered in OpenSees. The "bar" type only constrains the translational degree-of-freedom and "beam" type constrains both translational and rotational degrees of freedom. In this paper, the "beam" type constraint is used to model the full shear connection between the steel beam and concrete slab. A composite beam can be modeled in two alternative ways in OpenSees. One is to use a single section including steel I beam and concrete slab representing the composite beam. The other is to define the steel beam and slab separately with a rigid link connection between them to model the composite action.

3. FORMATION OF THE PROPOSED SHELL ELEMENT

3.1. Kinematics

A four-node isoparametric element is shown in Figure 3 for which bilinear shape functions N_i (Cook *et al*. 2002) are used to interpolate both coordinates and displacements of a generic point within the element from

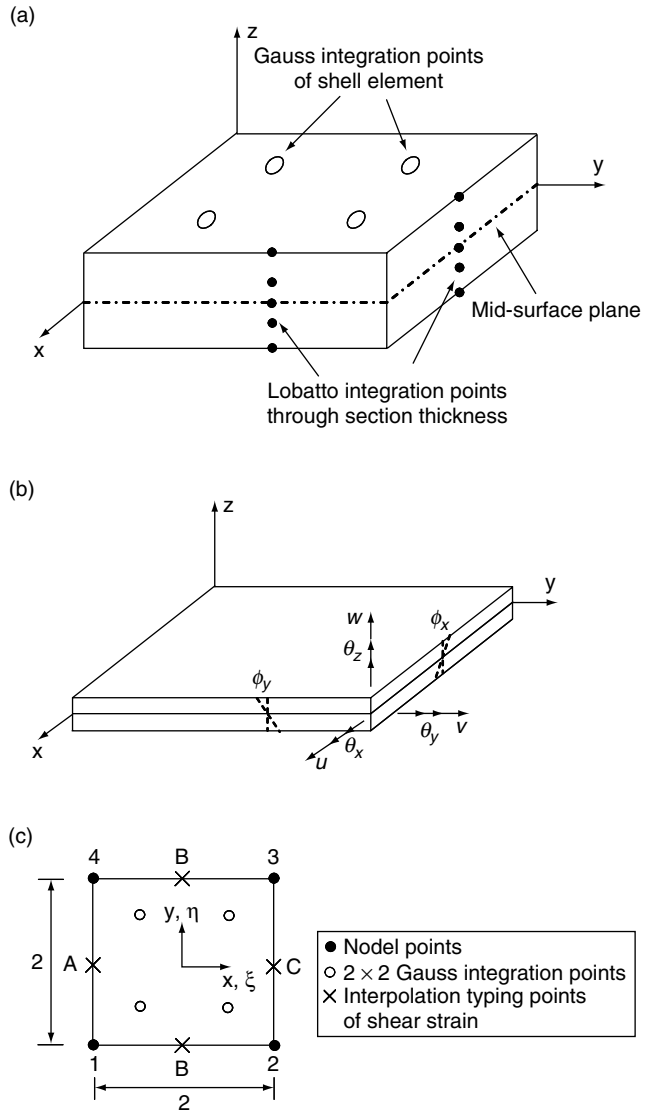

Figure 3. Geometry of a four-node shell element in the x, y plane: (a) Integration scheme of shell element; (b) Nodal degrees of freedom; (c) Geometry of 2 × 2 element

nodal coordinates and nodal displacements respectively, as shown in Eqns 1 and 2. The element has six degrees of freedom per node $\{u\ v\ w\ \theta_x\ \theta_y\ \theta_z\}^T$ (three translations u, v, w and three rotations θ_x, θ_y, θ_z as shown in Figure 4(b)).

$$x = \sum_{i=1}^{4} N_i x_i, \quad \text{and} \quad y = \sum_{i=1}^{4} N_i y_i \tag{1a}$$

$$u = \sum_{i=1}^{4} N_i u_i \ ; \ v = \sum_{i=1}^{4} N_i v_i \text{ and } w = \sum_{i=1}^{4} N_i w_i \tag{1b}$$

$$\theta_x = \sum_{i=1}^{4} N_i \theta_{xi} \ ; \ \theta_y = \sum_{i=1}^{4} N_i \theta_{yi} \text{ and } \theta_z = \sum_{i=1}^{4} N_i \theta_{zi} \tag{1c}$$

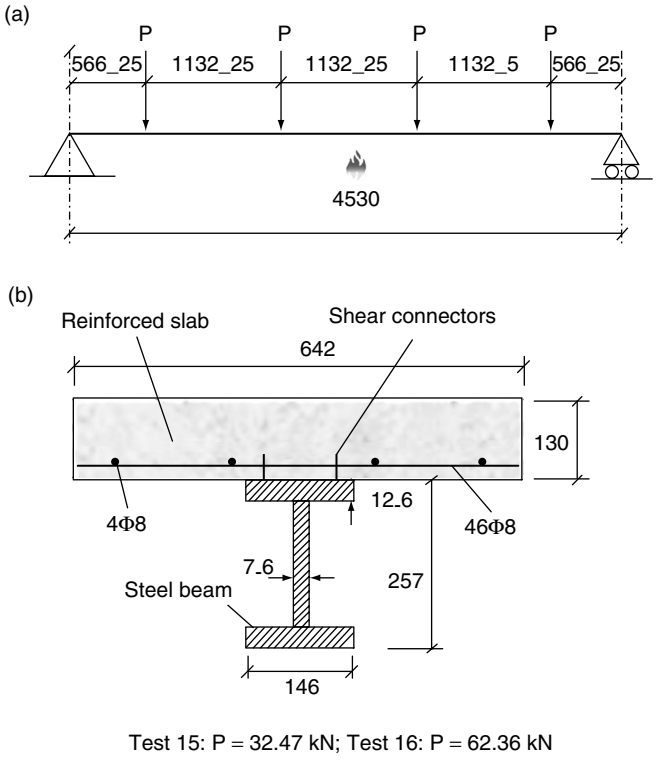

Figure 4. Schematic of tested composite beam (Test 15 and Test 16) (all dimensions in mm)

where N_i are the bilinear shape functions of the rectangular four-node element defined as

$$N_1 = \frac{(1-\xi)(1-\eta)}{4}; N_2 = \frac{(1+\xi)(1-\eta)}{4}; \\ N_3 = \frac{(1+\xi)(1+\eta)}{4}; N_4 = \frac{(1-\xi)(1+\eta)}{4} \tag{2}$$

Based on the Reissner-Mindlin plate theory, the displacement components u', v', w' of a generic point in the element with coordinates x, y, z can be expressed by their corresponding mid-surface displacements u, v, w and rotations ϕ_x, ϕ_y as

$$u'(x,y,z) = u(x,y) - z\phi_x(x,y); \\ v'(x,y,z) = v(x,y) - z\phi_y(x,y); \\ w'(x,y,z) = w(x,y). \tag{3}$$

where ϕ represents the rotation of the normal at the generic point to the mid-surface of the shell. It is convenient to use the physical rotation ϕ of a mid-surface normal to express the strain-displacement relation, which can be later transformed into θ by

$$\begin{Bmatrix} \phi_x \\ \phi_y \end{Bmatrix} = \begin{bmatrix} 0 & -1 \\ 1 & 0 \end{bmatrix} \begin{Bmatrix} \theta_x \\ \theta_y \end{Bmatrix} \tag{4}$$

A simplified Green strain can be expressed as

$$\varepsilon = \begin{Bmatrix} \varepsilon_x \\ \varepsilon_y \\ \gamma_{xy} \\ \gamma_{xz} \\ \gamma_{yz} \end{Bmatrix} = \begin{Bmatrix} u'_{,x} + \frac{1}{2}\left(w'_{,x}\right)^2 \\ v'_{,y} + \frac{1}{2}\left(w'_{,y}\right)^2 \\ u'_{,y} + v'_{,x} + w'_{,x}w'_{,y} \\ u'_{,z} + w'_{,x} \\ v'_{,z} + w'_{,y} \end{Bmatrix} \tag{5}$$

The membrane strain of a generic point in the shell element can be expressed as

$$\varepsilon^M = \begin{Bmatrix} \varepsilon_x \\ \varepsilon_y \\ \gamma_{xy} \end{Bmatrix} = \begin{Bmatrix} u_{,x} + \frac{1}{2}\left(w_{,x}\right)^2 - z\partial\phi_x/\partial x \\ v_{,y} + \frac{1}{2}\left(\overline{w}_{,y}\right)^2 - z\partial\phi_y/\partial y \\ u_{,y} + v_{,x} + w_{,x}w_{,y} - z\left(\partial\phi_x/\partial y + \partial\phi_y/\partial x\right) \end{Bmatrix} \tag{6}$$

where commas represent derivatives with respect to x or y.

Substituting the interpolation functions of displacements in Eqn 1, the membrane strain-displacement relationship can now be derived as

$$d\varepsilon^M = \sum_{i=1}^{4} \mathbf{B}_i^M d\mathbf{u}_i \tag{7}$$

in which $\mathbf{B}_i^M$ is the strain-displacement matrix,

$$\mathbf{B}_i^M = \begin{bmatrix} N_{i,x} & 0 & N_{i,x}N_{j,x}w_j & 0 & zN_{i,x} & 0 \\ 0 & N_{i,y} & N_{i,y}N_{j,y}w_j & -zN_{i,y} & 0 & 0 \\ N_{i,y} & N_{i,x} & \left(N_{i,x}N_{j,y} + N_{i,y}N_{j,x}\right)w_j & -zN_{i,x} & zN_{i,y} & 0 \end{bmatrix} \tag{8}$$

The Mixed Interpolation of Tensorial Components (MITC) technique (Dvorkin and Bathe 1984; Bathe and Dvorkin 1986) was used to form the shear strain to avoid the shear locking problems. The key formulation step is the replacement, in the potential energy principle, of selected displacement-related strains by independently assumed strain fields in element natural coordinates. The transverse shear strain was interpolated from the displacement-dependent strains defined at the mid-side of element edges as shown in Figure 4(c) as

$$\gamma = \begin{Bmatrix} \gamma_{\xi z} \\ \gamma_{\eta z} \end{Bmatrix} = \frac{1}{2}\begin{Bmatrix} (1-\eta)\gamma_{\xi z}^B + (1+\eta)\gamma_{\xi z}^D \\ (1-\xi)\gamma_{\eta z}^A + (1+\xi)\gamma_{\eta z}^C \end{Bmatrix} \tag{9}$$

where $\gamma_{\eta z}^A$, $\gamma_{\eta z}^C$ $\gamma_{\xi z}^A$, $\gamma_{\xi z}^D$ are the physical shear strains at points A, B, C, and D as shown in Figure 4(c). For the element shown in Figure 4, the MITC shear strain can be written as

$$\begin{aligned} \gamma_{\xi z} = {} & \frac{1}{2}(1-\eta)\left(\frac{w_2 - w_1}{2} - \frac{\phi_{x1} + \phi_{x2}}{2}\right) \\ & + \frac{1}{2}(1+\eta)\left(\frac{w_3 - w_4}{2} - \frac{\phi_{x3} + \phi_{x4}}{2}\right) \end{aligned} \tag{10a}$$

$$\begin{aligned} \gamma_{\eta z} = {} & \frac{1}{2}(1-\xi)\left(\frac{w_1 - w_4}{2} - \frac{\phi_{y1} + \phi_{y4}}{2}\right) \\ & + \frac{1}{2}(1+\xi)\left(\frac{w_3 - w_2}{2} - \frac{\phi_{y2} + \phi_{y3}}{2}\right) \end{aligned} \tag{10b}$$

Based on Eqn 9 the shear strain-displacement matrix can be defined as

$$d\gamma = \sum_{i=1}^{4} \mathbf{B}_i^S du_i \tag{11}$$

A combined strain-displacement matrix B can now be derived by assembly of membrane and shear components as

$$d\varepsilon = \begin{Bmatrix} d\varepsilon^M \\ d\gamma \end{Bmatrix} = \sum_{i=1}^{4} \begin{bmatrix} \mathbf{B}_i^M \\ \mathbf{B}_i^S \end{bmatrix} \mathrm{du}_i = \mathrm{Bdu} \tag{12}$$

The derivatives of the shape function with respect to x and y in strain-displacement matrix **B** are not available directly and they can be transformed from those with respect to ξ and η by Jocobian matrix [J] (Usmani *et al.* 2012) defined as

$$\begin{bmatrix} N_{i,x} \\ N_{i,y} \end{bmatrix} = [J]^{-1} \begin{bmatrix} N_{i,\xi} \\ N_{i,\eta} \end{bmatrix} \tag{13}$$

where

$$[J] = \begin{bmatrix} x_{,\xi} & y_{,\xi} \\ x_{,\eta} & y_{,\eta} \end{bmatrix} = \begin{bmatrix} \sum N_{i,\xi}x_i & \sum N_{i,\xi}y_i \\ \sum N_{i,\eta}x_i & \sum N_{i,\eta}y_i \end{bmatrix} \tag{14}$$

Drilling degrees of freedom (d.o.f.) are considered in the shell element. A drilling d.o.f. in a planar element is a rotational d.o.f. whose vector is normal to the plane of the element. Drilling d.o.f. can enhance the performance

of elements having only corner nodes compared with elements having both corner and side nodes. A fictitious stiffness k_θ is assigned to the drilling degree of freedom θ_z and it can be incorporated into the total potential energy using a penalty approach with k_θ being the penalty parameter.

$$\Pi_{drill} = \frac{1}{2}\int_V k_\theta \left(\omega - \theta_z\right)^2 dV \tag{15}$$

where ω is the physical in-plane rotation of shell defined as

$$\omega = \frac{1}{2}\left(v_{,x} - u_{,y}\right) \tag{16}$$

and the corresponding strain-displacement matrix can be written as

$$\mathrm{d}\left(\omega - \theta_z\right) = \mathrm{B}^{dr}\mathrm{du} \tag{17}$$

in which

$$\mathrm{B}^{dr} = \left[-\frac{1}{2}N_{i,y} \quad \frac{1}{2}N_{i,x} \quad 0 \quad 0 \quad 0 \quad -N_i\right] \tag{18}$$

So far the strain-displacement matrices are defined in the local coordinate system but it can be transformed into the global coordinate system by a transformation matrix before the calculation of the stiffness matrix (Cook *et al*. 2012).

3.2. Stress-Strain Relation

For isotropic elastic material, the stress-strain relation can be written as

$$\sigma = \left\{\sigma_x \quad \sigma_y \quad \tau_{xy} \quad \tau_{xz} \quad \tau_{yz}\right\}^T = [D]\left(\varepsilon - \varepsilon_T\right) \tag{19}$$

where [D] is the elasticity matrix; ε is the total strain calculated from the updated displacements of elements; ε_T is the thermal strain due to the temperature rise.

The stress is determined according to the mechanical strain which are obtained by subtracting the thermal strain from the total strain. The material nonlinearity in the plastic deformation can be considered by iteratively solving the equilibrium equations. A variety of solution algorithms such as Newton-Simpson method are available in OpenSees for static and dynamic analyses.

3.3. Element Stiffness Matrix

The total potential energy including the drilling rotation term can be written as

$$\Pi = \frac{1}{2}\int_V \varepsilon^T \sigma \mathrm{d}V + \frac{1}{2}\int_V k_\theta \left(\omega - \theta_z\right)^2 dV - \int_V u^T \mathrm{f}\mathrm{d}V \tag{20}$$

The first variation of Eqn 20 yields the governing equilibrium equation as

$$\begin{aligned}\delta\Pi = &\int_V \delta\varepsilon^T \sigma dV + \int_V \left(\delta\omega - \delta\theta_z\right)k_\theta\left(\omega - \theta_z\right)dV \\ &- \int_V \delta u^T f dV = 0\end{aligned} \tag{21}$$

By substituting the strain-displacement relationship of Eqn 12, Eqn 22 becomes

$$\int_V [B]\sigma dV + \left(\int_V \left[B^{dr}\right]^T k_\theta \left[B^{dr}\right] dV\right)u = \{F\} \tag{22}$$

Where $\{F\} = \int_V f dV$ is the equivalent elemental load.

Solutions of Eqn 22 must be iterative for geometrically nonlinear analysis, taking variation with respect to du we obtain

$$\begin{aligned}&\int_V d\left([B]^T \sigma\right)dV + \\ &\left(\int_V \left[B^{dr}\right]^T k_\theta \left[B^{dr}\right] dV\right) d\boldsymbol{u} = d\{F\}\end{aligned} \tag{23}$$

The first term of Eqn 23 can be expressed as

$$\int_V d\left([B]^T \sigma\right)dV = \int_V d[B]^T \sigma dV + \int_V [B]^T d\sigma dV \tag{24}$$

and together with the variation of stress in the form of

$$d\{\sigma\} = [D]d\{\varepsilon\} = [D][B]d\{u\} \tag{25}$$

Hence Eqn 23 becomes

$$\begin{aligned}&\int_V d[B]^T \sigma dV + \left(\int_V [B]^T [D][B] dV\right) \\ &du + \left(\int_V \left[B^{dr}\right]^T k_\theta \left[B^{dr}\right] dV\right) du = d\{F\}\end{aligned} \tag{26a}$$

Or

$$[K_T]du = d\{F\} \tag{26b}$$

where $F = \int_V f dV$ is the equivalent elemental load; $[K_T] = [K]^M + [K_\sigma] + [K]^D$ is the tangent stiffness matrix; $[K]^M = \int_V [B]^T [D][B] dV$ is the so-called material

matrix which is the function of initial geometry and displacement; $[K]^D = \int_V [B^{dr}]^T k_\theta [B^{dr}] dV$ is the additional "drilling stiffness" matrix. The corresponding strain-displacement matrix B^{dr} is defined by $d(\omega - \theta_z) = B^{dr}du$; $[K_\sigma]$ is known as geometric matrix defined as

$$\int_V d[B]^T \sigma dV = [K_\sigma] du \tag{27}$$

4. VALIDATION

4.1. Simply Supported Composite Beams under Mechanical and Fire Load

Two fire tests (Test 15 and Test 16) (Wainman and Kirby1988) were chosen to validate the performance of the proposed OpenSees model. The test set up and material properties are illustrated in Figure 4. The material class DruckerPragerThermal was used to model concrete slab and Steel01Thermal (Jiang and Usmani 2013) for modeling the steel beam. Figure 5 shows the comparisons of OpenSees results and experimental data which show reasonable agreement.

4.2. Cylindrical Bending of Plain Concrete Slabs

The plate is assumed to have infinite extent in the y direction with loading and support conditions independent of y. The two edges along the y direction are restrained in lateral translation (in the x direction) but free to rotate about the y axis. They are also free to translate along the y direction. The plate is subjected to a uniformly distributed load (UDL) and a uniform temperature increase. An equivalent strip can be cut from the plate, as shown in Figure 6. The restraint force P is produced by the combined effects of restrained thermal expansion and large deflections. With q being the intensity of the UDL, the equilibrium equation governing the bending of the plate can be written as

$$\frac{d^2w}{dx^2} + \frac{Pw}{D} = -\frac{qax}{2D} + \frac{qx^2}{2D} \tag{28}$$

where $D = Et^3/12(1-\nu^2)$ is the bending stiffness of the plate; E is the modulus of elasticity; t is the thickness of the plate and ν is the Poisson ratio.

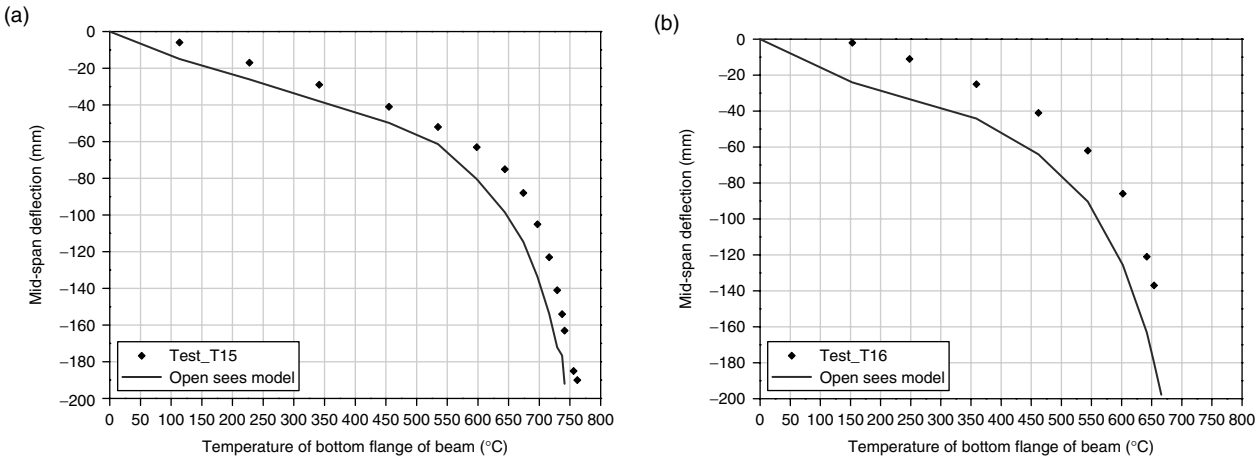

Figure 5. Comparison of measured and predicted mid-span deflection of tested beams: (a) beam Test 15; (b) beam Test 16

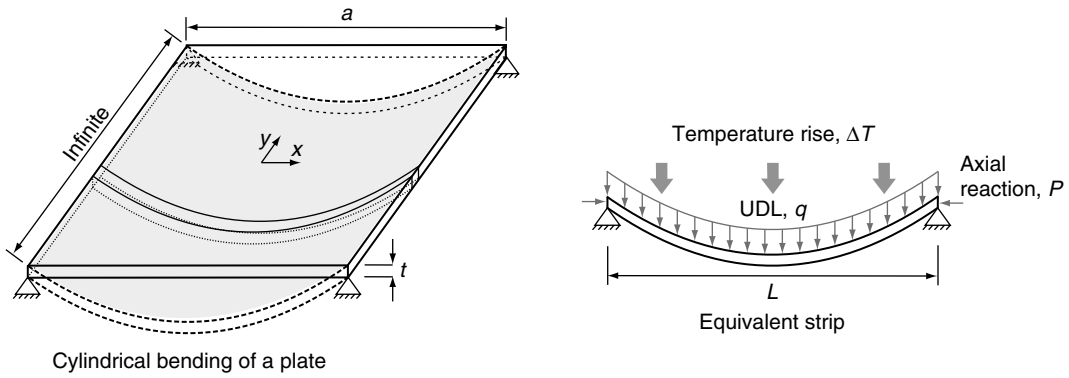

Figure 6. Schematic view of cylindrical bending of a rectangular plate

Introducing the notation

$$k = \sqrt{\frac{P}{D}} \tag{29}$$

the general solution of Eqn 28 can be written in the following form:

$$w = C_1 \sin kx + C_2 \cos kx + \frac{q}{2Dk^2}x^2 - \frac{qa}{2Dk^2}x - \frac{q}{Dk^4} \tag{30}$$

The constants of C_1 and C_2 can be determined from the boundary conditions and the solution of deflection w becomes

$$w = \frac{q}{Dk^4}\left[\frac{1-\cos ka}{\sin ka}\sin kx + \cos kx - 1\right] + \frac{q}{2Dk^2}x^2 - \frac{qa}{2Dk^2}x \tag{31}$$

The mid-span deflection can be derived from Eqn 31 as

$$w_{mid} = \frac{q}{Dk^4}\left[\frac{1-\cos ka}{\sin ka}\sin\left(\frac{ka}{2}\right) + \cos\left(\frac{ka}{2}\right) - 1\right] - \frac{qa^2}{8Dk^2} \tag{32}$$

To solve Eqn 32, the axial force P should be determined first. However, P is also a function of the deflection w since it results from the combined effects of restrained thermal expansion and extension developed in the strip due to the large deflection.

The extension of the strip produced by the deflection w is equal to the difference between the length of the arc a_{arc} along the deflection curve and the chord length a. If the sin curve of deformation shape is assumed, the mid-span deflection can be calculated as (Usmani *et al.* 2001)

$$w_{mid} = \frac{2a}{\pi}\sqrt{\varepsilon_w + \frac{\varepsilon_w^2}{2}} \tag{33}$$

where $\varepsilon_w = \dfrac{a_{arc} - a}{a}$ is the tensile strain and can be expressed in turn as

$$\varepsilon_w = \sqrt{\frac{1}{2}\left(\frac{\pi w_{mid}}{a}\right)^2 + 1} - 1 \tag{34}$$

The horizontal reaction force in the support can be written as

$$P = EA\left[\varepsilon_T - \varepsilon_w\right] \tag{35}$$

where ε_T is the thermal elongation $\varepsilon_T = \alpha\Delta T$ and A is cross section area per unit length.

A 6 m × 6 m steel plate with a thickness of 200 mm was modelled in OpenSees. An elastic material with a modulus of elasticity of 200GPa and Poisson's ratio of 0.3 was assumed for the steel. The steel plate was subjected to a uniformly distributed load of 1000 kN/m^2. A constant thermal expansion coefficient of 12×10^{-6}/°C was assumed for this problem. Figure 7 shows the comparison of analytical and OpenSees results. As can be seen, the OpenSees results are in good agreement with the analytical results. The infinite length edge was considered to be 30 m long in OpenSees and a constant E was used. The analytical results were derived by iteratively solving Eqns 32 and 35. The horizontal reactions derived from OpenSees was not uniformly distributed along the edge as shown in Figure 9

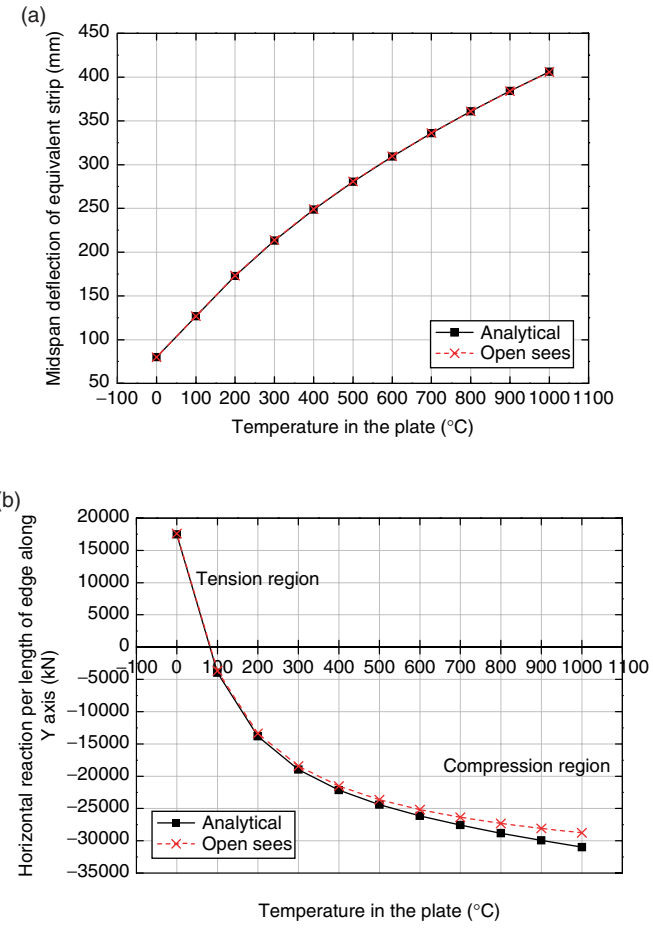

Figure 7. Response of cylindrical bending of uniformly heated plates: (a) mid-span deflection; (b) reaction at restraint

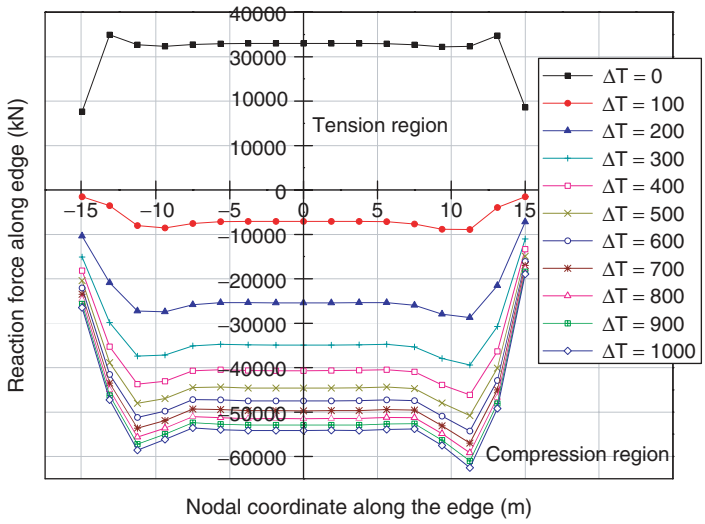

Figure 8. Horizontal reaction distribution along the edge in the y direction

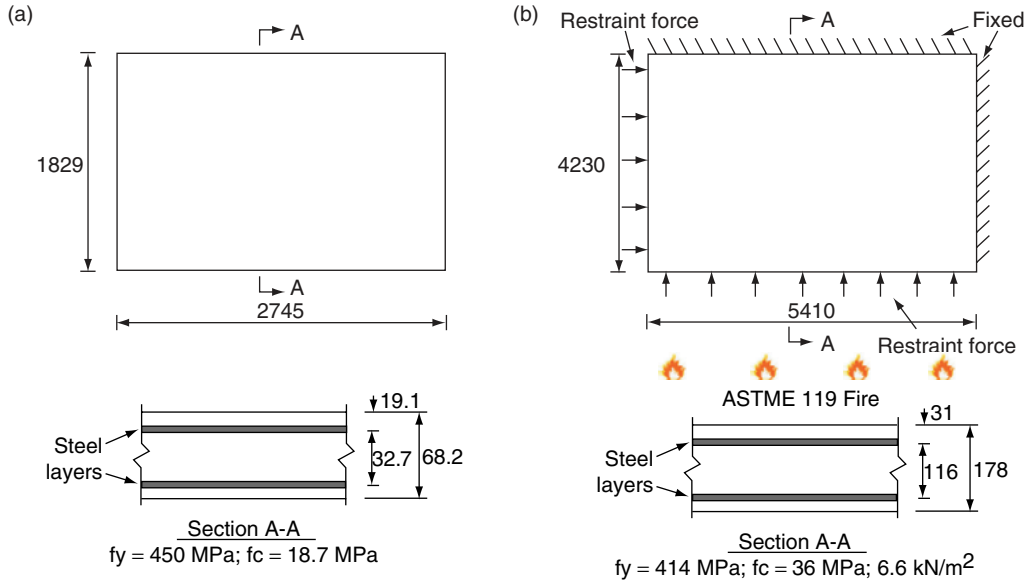

Figure 9. Details of test specimens modeled in OpenSees: (a) specimen B1; (b) specimen S-56

therefore the average values are used to compare with the analytical solution. It was also found, from Figures 7(b) and 8, that the increments of the reaction slowed down as the temperature increased which may be driven by the increasing catenary action due to the extension of the strip under large deflection.

4.3. Two-Way Bending of Reinforced Concrete Slabs

In this section two test specimens of reinforced concrete slabs were modelled in OpenSees to check its performance for simulating membrane action. One specimen, denoted B1, was a rectangular slab tested by Ghoneim and MacGregor (1994a, b) subjected to a uniformly distributed load (UDL) perpendicular to the plane of the plate, of which overall dimensions were 2,745 mm × 1,829 mm with a thickness of 68.2 mm. A comparison has also been made with a flat reinforced concrete slab (S-56) exposed to the ASTM E119 fire (Lin *et al.* 1989). The geometric dimensions of the specimen S-56 were 5,410 mm × 4,230 mm with a thickness of 178 mm. Another interesting feature of this test was thatits thermal expansion was resisted by jacks in order to simulate behaviors found in a real structure (Lin *et al.* 1989). The compressive strength of the concrete and yield strength of the steel were 36 MPa and 414 MPa, respectively. The measured details of the geometry of the specimens B1 and S-56, with the

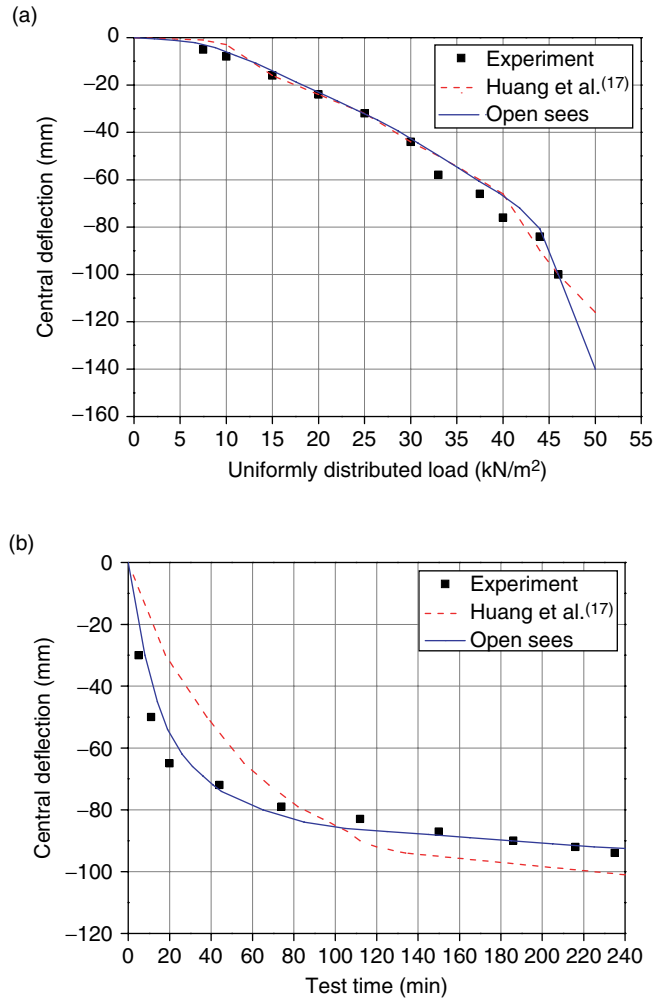

Figure 10. Comparison of predicted and measured central deflections: (a) specimen B1; (b) specimen S-56

positions of reinforcement layers, are shown in Figure 9. The central deflections measured from the test and predicted by OpenSees as well as Huang *et al*. (2003b) are plotted in Figure 10. The predicted results from OpenSees are in good agreement with test results. The distributions of the two principal membrane tractions within the plate B1 are shown in Figure 11. It can be seen that high compressive membrane tractions are formed at the edges of the plate, which equilibrate the biaxial tensile membrane tractions within the central zone carried mainly by the steel reinforcement.

4.4. Cardington Restrained Beam Test

The restrained beam test (British Steel 1999) was carried out on the 7th floor of the composite steel framed structure at Cardington shown in Figure 12(a). A beam (305 × 165 × 40UB) was heated over the middle 8.0 m of its 9.0 m length keeping the connections as close as possible to ambient temperature. A three-dimensional model of the Cardington restrained beam test was built in OpenSees as

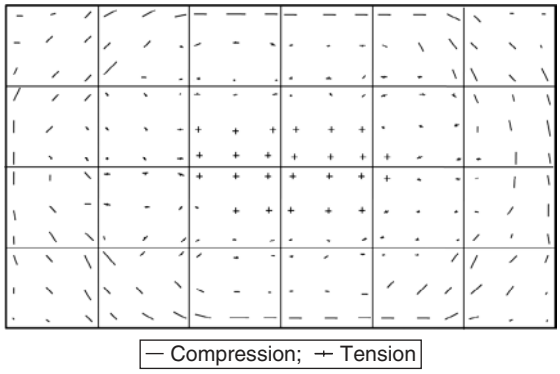

Figure 11. Distributions of the two principal membrane tractions at Gauss points for specimen B1

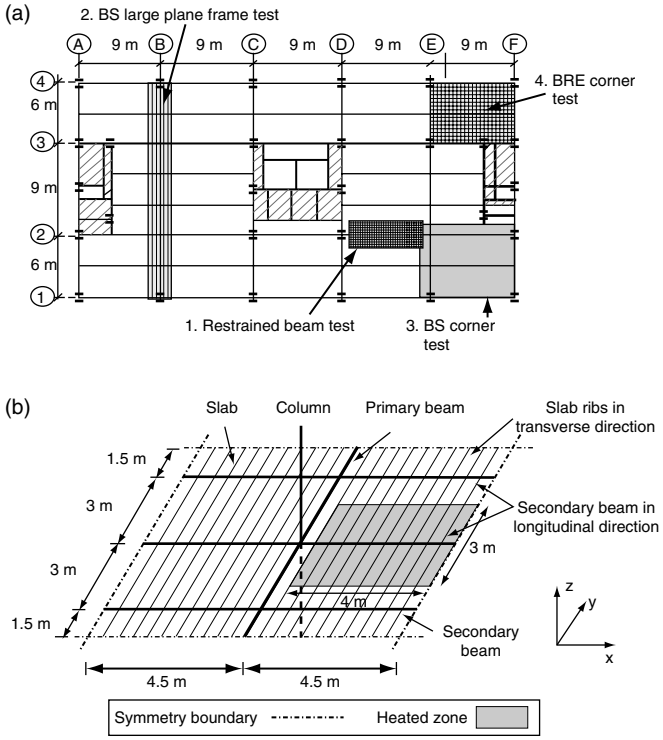

Figure 12. Geometric model of the restrained beam test: (a) test set up (BS 1999); (b) OpenSees model

shown in Figure 12(b). Exploiting symmetry, only half the compartment was modeled and the effect of the surrounding floor was also represented by symmetry boundary conditions. The model consisted of flat slab, concrete ribs and a primary beam in the transverse direction, a column in the middle and the heated (restrained) beam in the longitudinal direction as well as the other two parallel secondary beams. The profiled deck slab was modeled separately by shell elements ShellMITC4GNThermal representing the flat reinforced concrete slab and 3D beam elements DispBeamColumn3DThermal representing the concrete ribs. The 3D beam element DispBeamColumn3DThermal

was also used for modeling the column and beams. The slab, ribs, column and beams were connected using the rigid link element. The extent of the column modeled was the full length from one floor below the floor on which the test took place to one floor above it. The bottom end of the column was fully fixed whilst at the top only vertical deflection were permitted. The mesh of this restrained beam test model in OpenSees is shown in Figure 13. A 30 × 18 element mesh was used in the x and y direction of the slab respectively with 16 elements for the column. The compressive strength of concrete is 48 MPa and the yield stress of steel is 280 MPa. The material class DruckerPragerThermal was used to model the concrete in slab and Concrete02Thermal (Jiang and Usmani 2013) for the concrete in the ribs. Steel01Thermal (Jiang and Usmani 2013) was used to model the steel I beam and reinforcement in the ribs. The reinforcement in the slab was modeled by a smeared layer distributed in the shell elements.

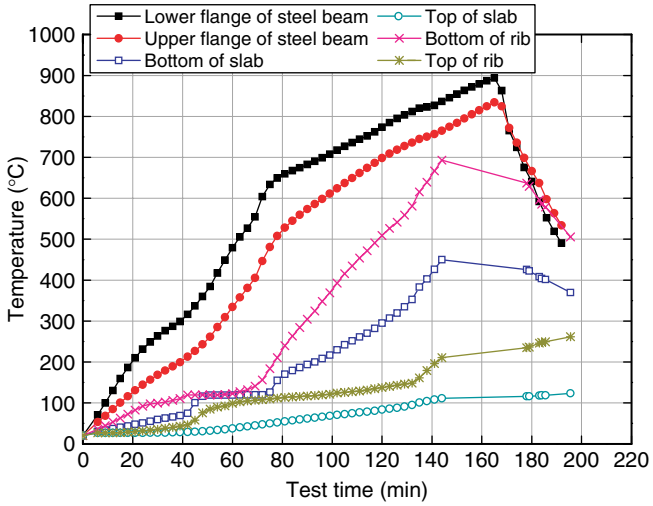

Figure 13. Temperature distribution in the composite slab of restrained beam test

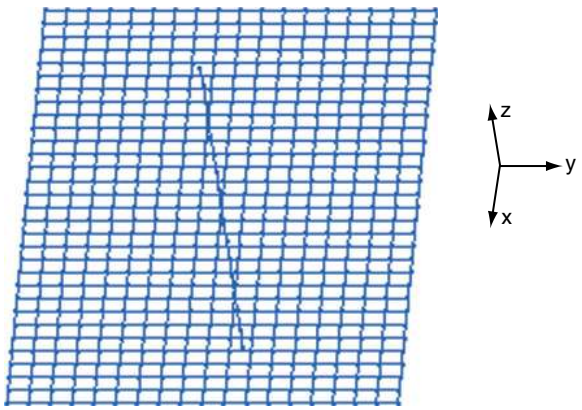

Figure 14. Mesh of Cardington restrained beam model in OpenSees

A uniformly distributed load of 5.48 kN/m^2 (Gillie *et al*. 2002) was applied over the entire floor slab and the temperature profile was shown in Figure 13. The loading was applied in two stages. First the static load was applied while the structure was unheated. The structure was then heated according to the recorded test temperature-time curves while keeping the static load constant. Nonlinear dynamic analysis was carried out in OpenSees. Newmark method with $\gamma = 0.45$ and $\beta = 0.8$ and Newton-Raphson solution algorithm were applied.

Figure 15 shows the deformed shape of the 3D model in OpenSees after 120 minutes. Figures 16 and 17 show the mid-span deflection of the restrained beam and the horizontal displacement of the column at floor level respectively. Reasonable agreements were achieved. It is interesting to see that there is a plateau in the horizontal displacement of column as shown in Figure 17. As temperature rises, the horizontal displacement of the column increases until about 250 ºC and stays almost unchanged until 500 ºC after which it begins to increase again. The initial increase is primarily due to the thermal expansion of the steel beam. The steel beam bottom flange yields at 250 ºC which reduces the increase inrestraint to thermal expansion resulting in the plateau in Figure 17, which is picked up in a qualitative sense by the OpenSees model. The midspan deflection carries on increasing during the plateau stage because of the thermal bowing induced by the increasing thermal gradient in the composite system. The second part of the increase in the column horizontal displacement is due to the thermal expansion of the concrete slab which heats up less rapidly than the beam as shown in Figure 13.

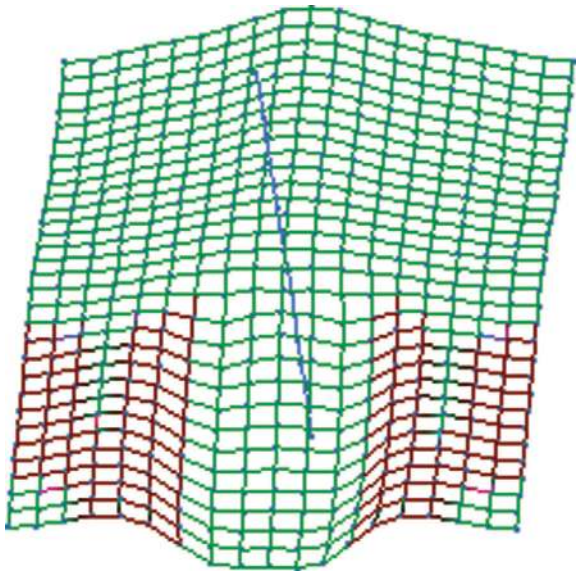

Figure 15. Deformed shape of Cardington restrained beam model in OpenSees (×100)

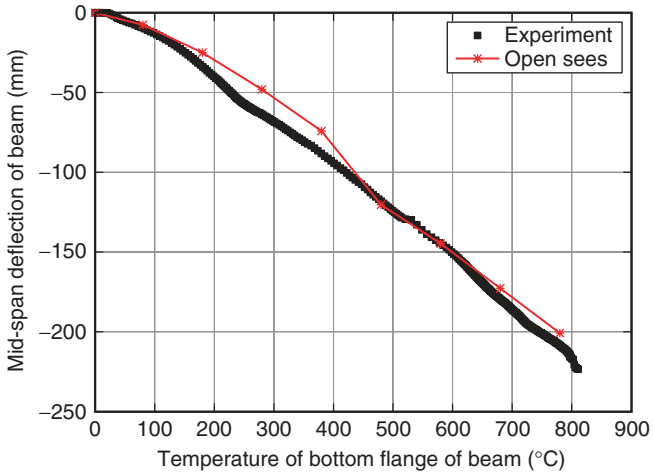

Figure 16. Mid-span deflection of the restrained beam against temperature

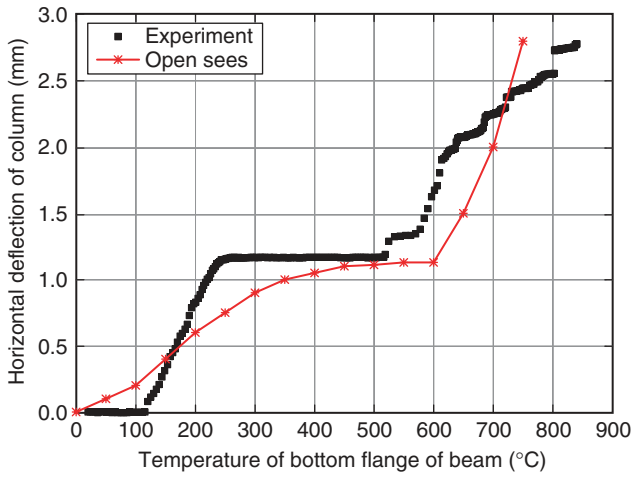

Figure 17. Horizontal displacement of the column against temperature

4.5. Cardington Corner Test

The British Steel corner test (1999) was carried out on the first floor in a compartment 10m wide by 7.5 m deep with a floor area of approximately 80 m^2 as shown in Figure 12(a). The whole corner compartment was modelled in OpenSees and the effect of the surrounding floor was also represented by symmetry boundary conditions (as shown in Figure 18). The same external load and material and element classes were used to model the slab, ribs, beams and columns as for the restrained beam test model described earlier. The mesh of this corner test model in OpenSees is shown in Figure 19. A 45 × 15 element mesh was used in the x and y direction of the slab respectively and 16 elements were used for the column.

Figure 21 shows the deformed shape of the 3D model in OpenSees after 80 minutes. The temperature

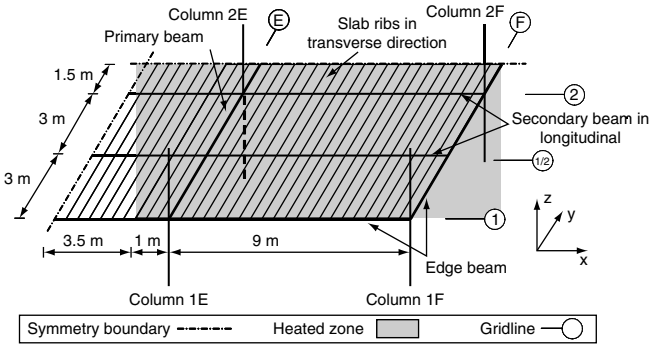

Figure 18. Geometric model of the restrained beam test

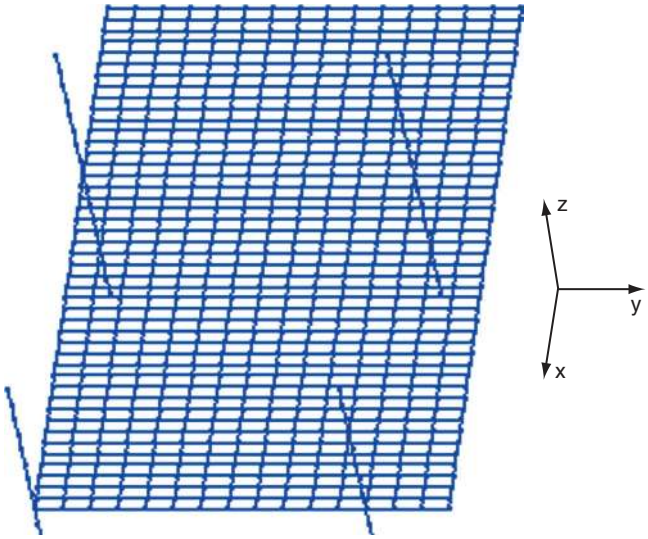

Figure 19. Mesh of Cardington corner test model in OpenSees

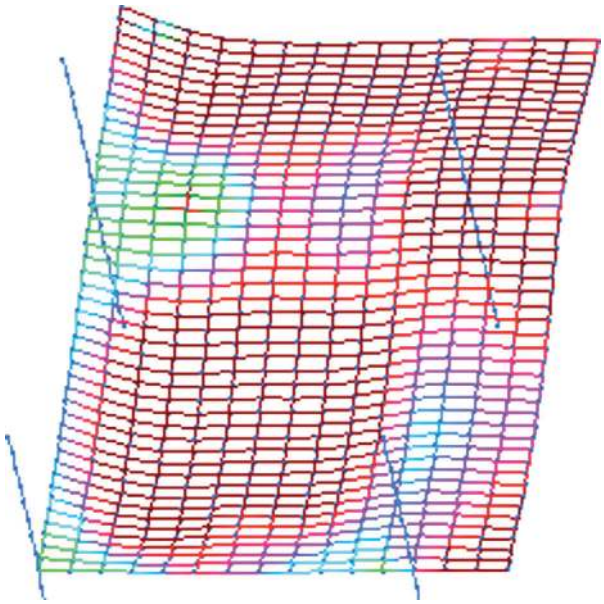

Figure 20. Deformation shape of Cardington restrained beam model in OpenSees (×100)

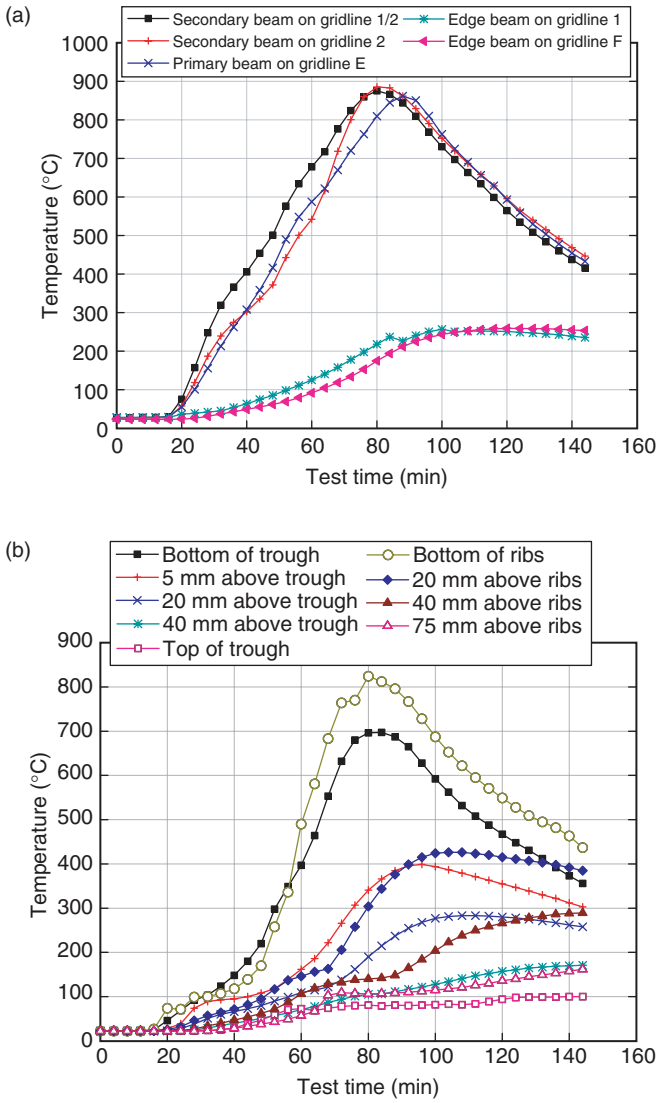

Figure 21. Temperature distribution of the corner test: (a) Temperature distribution in the beam; (b) Temperature distribution in the slab

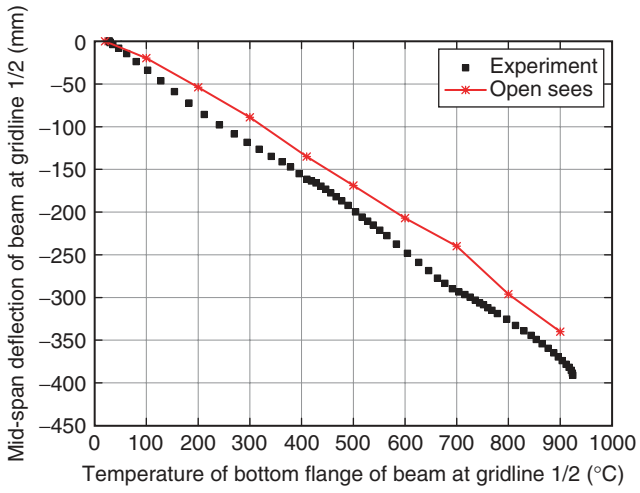

Figure 22. Mid-span deflection of the secondary beam against temperature

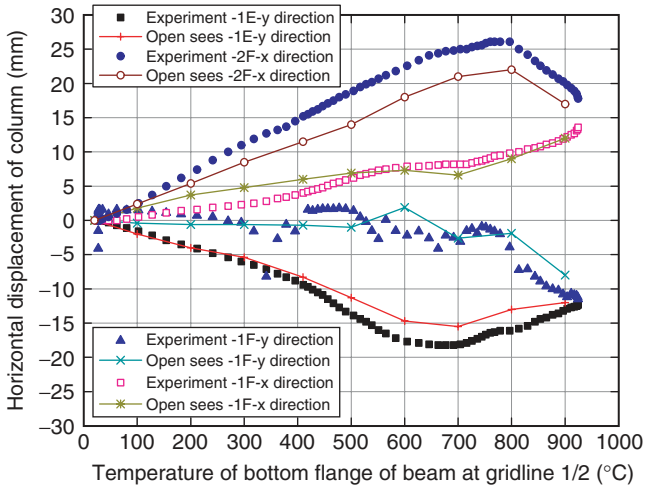

Figure 23. Horizontal displacement of the columns against temperature

distributions in the structural components are shown in Figure 21. The mid-span deflection of the beam at gridline 1/2 and horizontal displacement of the four columns (column 1E, 2E, 1F and 2F) are shown in Figures 22 and 23 respectively. The horizontal displacement of column 1E in the y direction is larger than that of column 1F and this is because the temperature in the beam on gridline E is higher than that of the beam on gridline F. Similarly, the horizontal displacement of column 2F in the x direction is larger than that of column 1F because of higher temperature in the beam on gridline 2. The OpenSees results agree well with the experiment results.

This sort of comparison is usually very difficult to make because of the difficulties of representing the complex realities of a real test structure, particularly with a relatively simple model such as this (which is perhaps the reason why such comparisons have never been reported in any other papers on modelling the Cardington tests except Gillie et al. 2001, 2002). It can therefore be concluded with reasonable confidence that OpenSees has been validated for steel framed composite structures subjected to fire.

5. CONCLUSIONS

The OpenSees framework has been extended to model steel framed composite structures exposed to fire. The following conclusions may be drawn:

(1) A layered geometrically and materially nonlinear shell element was proposed in this paper where the MITC technique and drilling degrees of freedom are included to enhance the element's overall performance. Its ability to

simulate membrane action in reinforced concrete slabs was validated.

(2) The performance of the new code developed for modeling composite structures in fire in OpenSees was extensively verified and validated against analytical and experimental results. Adequate quantitative agreements are achieved between OpenSees predictions and experimental measurements.

(3) The difficult "plateau" feature in the column horizontal displacement in the Cardington restrained beam test was adequately simulated in OpenSees suggesting that complex physical phenomena witnessed in real experiments can be captured using relatively simple structural models.

(4) The horizontal movement of columns in the Cardington corner test was modeled and was found to be dominated by the thermal expansion of composite beams. The largest displacement was observed in the column nearest to the corner column which was pushed out first due to the expansion of the heated steel beams followed by pulling in because of thermal bowing of the composite slab and the tensile forces generated by catenary effect of the heated beam under large deflections. No simulations of the Cardington corner test reported in the literature so far match the quality of these results.

ACKNOWLEDGEMENTS

The work presented in this paper was supported by the National Natural Science Foundation of China with grant 51120185001 as well as China Postdoctoral Science Foundation (2013M531216). The contributions from Panagiotis Kotsovinos are gratefully acknowledged.

REFERENCES

Archer, G.C., Fenves, G. and Thewalt, C. (1999). "A new object-oriented finite element analysis program architecture", *Computers & Structures*, Vol. 70, No. 1, pp. 63–75.

Bailey, C.G. (1995). *Simulation of the Structural Behavior of Steel-Framed Buildings in Fire*, PhD Thesis, Department of Civil and Structural Engineering, University of Sheffield, UK.

Bathe, K.J. and Dvorkin, E. (1986). "A formulation of general shell elements- the use of mixed interpolation of tensorial components", *International Journal for Numerical Methods in Engineering*, Vol. 22, No. 3, pp. 697–722.

British Steel (BS) plc. (1999). *The Behaviour of Multi-Storey Steel Framed Buildings in Fire*, Report of British Steel, Swinden Technology Center, UK.

Chen, W.F. and Saleeb, A.F. (1994). *Constitutive Equations for Engineering Materials Volume I: Elasticity and Modeling*, Elsevier Science B.V., Amsterdam.

Cook, R.D., Malkus, D.S., Plesha, M.E. and Witt, R.J. (2002). *Concepts and Applications of Finite Element Analysis*, 4th Edition, John Wiley and Sons publishers.

Dong, Y.L., Zhu, E.C. and Prasad, K. (2009). "Thermal and structural response of two-storey two-bay composite steel frames under furnace loading", *Fire Safety Journal*, Vol. 44, No. 4, pp. 439–450.

Drucker, D.C. and Prager, W. (1952). "Soil mechanics and plastic analysis for limit design", *Quarterly of Applied Mathematics*, Vol. 10, No. 2, pp. 157–165.

Dvorkin, E.N. and Bathe, K.J. (1984). "A continuum mechanics based four-node shell element for general nonlinear analysis", *Engineering with Computers*, Vol. 1, No. 1, pp. 77–88.

Elghazouli, A.Y., Izzuddin, B.A. and Richardson, A.J. (2000). "Numerical modelling of the structural fire behaviour of composite buildings", *Fire Safety Journal*, Vol. 35, No. 4, pp. 279–297.

Elghazouli, A.Y. and Izzuddin, B.A. (2001). "Analytical assessment of the structural performance of composite floors subject to compartment fires", *Fire Safety Journal*, Vol. 36, No. 8, pp. 769–793.

Eurocode 2 (2005). *Design of Concrete Structures: Part 1.2: General Rules, Structural Fire Design*, European Committee for Standardisation, Brussels, Belgium.

Franssen, J.M., Kodur, V.K.R. and Mason, J. (2000). *User's Manual for SAFIR2001*, A computer program for analysis of structures submitted to the fire, University of Liege, Belgium.

Ghoneim, M.G. and MacGregor, J.G. (1994a). "Tests of reinforced concrete plates under combined in-plane and lateral loads", *ACI Structural Journal*, Vol. 91, No. 1, pp. 19–30.

Ghoneim, M.G. and MacGregor, J.G. (1994b). "Behavior of reinforced concrete plates under combined in-plane and lateral loads", *ACI Structural Journal*, Vol. 91, No. 2, pp. 188–197.

Gillie, M., Usmani, A.S. and Rotter, J.M. (2001). "A structural analysis of the first cardington test", *Journal of Constructional Steel Research*, Vol. 57, No. 6, pp. 581–601.

Gillie, M., Usmani, A.S. and Rotter, J.M. (2002). "A structural analysis of the cardington british steel corner test", *Journal of Constructional Steel Research*, Vol. 58, No. 4, pp. 427–443.

Guo, S. and Bailey, C.G. (2011). "Experimental behaviour of composite slabs during the heating and cooling fire stages", *Engineering Structures*, Vol. 33, No. 2, pp. 563–571.

Guo, S. (2012). "Experimental and numerical study on restrained composite slab during heating and cooling", *Journal of Constructional Steel Research*, Vol. 69, No. 1, pp. 95–105.

Huang, Z., Burgess, I.W. and Plank, R.J. (1999). "Nonlinear analysis of reinforced concrete slabs subjected to fire", *ACI Structural Journal*, Vol. 96, No. 1, pp. 127–35.

Huang, Z., Burgess, I.W. and Plank, R.J. (2000a). "Non-linear modelling of three full scale structural fire tests", *Proceedings of the First International Workshop on Structures in Fire*, Copenhagen, Denmark.

Huang, Z., Burgess, I.W. and Plank, R.J. (2000b). "Effective stiffness modelling of composite concrete slabs in fire", *Engineering Structures*, Vol. 22, No. 9, pp. 1133–1144.

Huang, Z., Burgess, I.W. and Plank, R.J. (2000c). "Three-dimensional analysis of composite steel-framed buildings in fire", *Journal of Structural Engineering*, ASCE, Vol. 126, No. 3, pp. 389–397.

Huang, Z., Burgess, I.W. and Plank, R.J. (2003a). "Modelling membrane action of concrete slabs in composite buildings in fire — Part I: Theoretical development", *Journal of Structural Engineering*, ASCE, Vol. 129, No. 8, pp. 1093–1102.

Huang, Z., Burgess, I.W. and Plank, R.J. (2003b). "Modelling membrane action of concrete slabs in composite buildings in fire — Part II: Validations", *Journal of Structural Engineering*, ASCE, Vol. 129, No. 8, pp. 1103–1112.

Huang, Z., Burgess, I.W. and Plank, R.J. (2004). "Fire resistance of composite floors subject to compartment fires", *Journal of Constructional Steel Research*, Vol. 60, No. 2, pp. 339–360.

Huang, Z. (2010). "The behaviour of reinforced concrete slabs in fire", *Fire Safety Journal*, Vol. 45, No. 5, pp. 271–282.

Izzuddin, B.A. (1991). *Nonlinear Dynamic Analysis of Framed Structures*, PhD Thesis, Imperial College, University of London, London, UK.

Izzuddin, B.A., Tao, X.Y. and Elghazouli, A.Y. (2004). "Realistic modelling of composite and R/C floor slabs under extreme loading-Part I: Analytical method", *Journal of Structural Engineering*, ASCE, Vol. 130, No. 12, pp. 1972–1984.

Jiang, J. (2012). *Nonlinear Thermomechanical Analysis of Structures using OpenSees*, PhD Thesis, University of Edinburgh, Edinburgh, UK.

Jiang, J., Jiang, L.M., Kotsovinos, P., Zhang, J., Usmani, A.S., McKenna, F. and Li G.Q. (2013a). "OpenSees software architecture for the analysis of structures in fire", *Journal of Computing in Civil Engineering*, ASCE. (in press)

Jiang, J. and Usmani, A.S. (2013b). "Modeling of steel frame structures in fire using OpenSees", *Computers & Structures*, Vol. 118, pp. 90–99.

Lamont, S., Usmani, A.S. and Gillie, M. (2004). "Behaviour of a small composite steel frame structure in a "long-cool" and a "short-hot" fire", *Fire Safety Journal,* Vol. 39, No. 5, pp. 327–357.

Lin, T.D., Zwiers, R.I., Shirley, S.T. and Burg, R.G. (1989). "Fire test of concrete slab reinforced with epoxy-coated bars", *ACI Structural Journal*, Vol. 86, No. 2, pp. 156–162.

Mazzoni, S., McKenna, F., Scott, M.H. and Fenves, G.L. (2007). *OpenSees Command Language Manual*, University of California, Berkeley.

McKenna, F.T. (1997). *Object-Oriented Finite Element Programming: Frameworks for Analysis, Algorithms and Parallel Computing*, PhD Thesis, University of California, Berkeley, California, USA.

McKenna, F., Scott, M.H. and Fenves, G.L. (2010). "Nonlinear finite-element analysis software architecture using object composition", *Journal of Computing in Civil Engineering*, ASCE, Vol. 24, No. 1, pp. 95–107.

Rose, P.S., Bailey, C.G., Burgess, I.W. and Plank, R.J. (1998). "The influence of floor slabs on the structural performance of the Cardington frame in fire", *Journal of Constructional Steel Research*, Vol. 46, No. 1, pp. 310–311.

Sanad, A.M., Rotter, J.M., Usmani, A.S. and O'Connor, M. (2000). "Composite beams in large buildings under fire-numerical modeling and structural behaviour", *Fire Safety Journal*, Vol. 35, No. 3, pp. 165–188.

Sharma, U.K., Bhargava, P. and Singh, B. (2012). "Full-scale testing of a damaged reinforced concrete frame in fire", *Structures and Buildings*, Vol. 165, No. 7, pp. 335–346.

Spacone, E. and Filippou, F.C. (1992). *A Beam Element for Seismic Damage Analysis,* Report, University of California, Berkeley, California, USA.

Usmani, A.S. (2000). "Application of fundamental structural mechanics principles in assessing the cardington fire tests", *Proceedings of the First International Workshop on Structures in Fire*, Copenhagen, Denmark.

Usmani, A.S., Rotter, J.M., Lamont, S., Sanad, A.M. and Gillie, M. (2001). "Fundamental principles of structural behaviour under thermal effects", *Fire Safety Journal*, Vol. 36, No. 8, pp. 721–744.

Usmani, A.S., Zhang, J., Jiang, J., Jiang, Y.Q. and May, I. (2012). "Using OpenSees for structures in fire", *Journal of Structural Fire Engineering*, Vol. 3, No. 1, pp. 57–70.

Wainman, D.E. and Kirby, B.R. (1988). *Compendium if UK Standard Fire Test Data Unprotected Structural Steel-1*, British Steel Corporation, Ref. No. RS/RSC/S10328/1/98/B, Swinden Laboratories, Rotherdam.

Yu, X.M., Huang, Z., Burgess, I.W. and Plank, R.J. (2008). "Nonlinear analysis of orthotropic composite slabs in fire", *Engineering Structures*, Vol. 30, No. 1, pp. 67–80.